

# Improved Seventh-Order WENO Scheme

Yiqing Shen\* Gecheng Zha†

Dept. of Mechanical and Aerospace Engineering

University of Miami

Coral Gables, Florida 33124

E-mail: yqshen@miami.edu, gzha@miami.edu

## Abstract

In this paper, an improved seventh-order WENO (WENO-Z7) scheme is suggested by extending the 5th-order WENO scheme of Borges et al [R. Borges, M. Carmona, B. Costa, W. S. Don, An improved weighted essentially non-oscillatory scheme for hyperbolic conservation laws, *J. Comput. Phys.* 227(2008) 3191-3211]. The sufficient condition for seventh-order accuracy is described for the new smoothness indicator. The role of the parameter  $\varepsilon$ , which is used to construct the weights of WENO schemes to prevent the denominator from being zero, is discussed, and an optimized value of  $\varepsilon$  is suggested to improve the convergence and accuracy for practical applications.

## 1 Introduction

The WENO scheme concept was first proposed by Liu et al [1] and then improved by Jiang and Shu [2]. WENO schemes are based on ENO (essentially non-oscillatory) schemes [3, 4], but use a convex combination of all candidate stencils instead of the smoothest one in the ENO schemes. The WENO schemes achieve high order accuracy in smooth regions with more compact stencil and have better convergence due to the smoother numerical flux used.

There are two areas that are active for WENO schemes development. The first area is to improve the ENO properties. For example, Wang and Chen [5] proposed optimized WENO schemes for linear waves with discontinuity; Panziani et al [6] developed the optimized WENO schemes to improve the resolution of a class of compressible flows characterized by a wide disparity of scales for compressible turbulence and/or aeroacoustic phenomena, and shock waves; Balsara and Shu [7] developed the monotonicity preserving WENO schemes; Xu and Shu [8] generalized a technique of anti-diffusive flux corrections to WENO schemes. Henrick et al [9] pointed out that the original smoothness indicators of Jiang and Shu fail in improving the accuracy order of WENO scheme at a critical point, where the first order derivatives is zero. A mapping function is proposed by Henrick et al [9] to obtain the optimal order near critical points. Borges et al [10] devised a new set of WENO weights that satisfies the necessary and sufficient conditions for fifth-order convergence proposed by Henrick et al [9] and enhances the accuracy at critical points. Shen and Zha [11] found that most of the WENO schemes do not achieve the optimal accuracy near discontinuities. They introduced fourth-order fluxes to overcome this drawback. A class of higher than 5th order weighted essentially non-oscillatory schemes are designed by Balsara and Shu in [7]. Martin et al [12] proposed a symmetric WENO method by means of a new candidate stencil. Their schemes are  $2r$ th-order accurate and symmetric, and less dissipative than Jiang and Shu's scheme.

---

\* Research Scientist, AIAA Member

† Associate Professor, AIAA Senior Member

The second area is to combine WENO with other high order schemes, for example, Pirozzoli[13] proposed a hybrid compact-WENO scheme for shock-turbulence interaction; Kim and Kwon[14] proposed a high-order accurate hybrid scheme using a central flux scheme and a WENO scheme for compressible flow-field analysis, Shen and Yang[15] developed hybrid finite compact-WENO schemes. Costa and Don[16, 17] developed hybrid central-WENO and hybrid spectral-WENO methods.

During the application of fifth-order WENO schemes, Shen et al[18] observed that a too small  $\varepsilon$  used in WENO schemes will cause convergence instability problem due to the oscillation of the weights, even in the smooth regions. Furthermore, the weights are deviated from the optimal weights and hence introduce numerical dissipation.

In this paper, an improved seventh-order WENO (WENO-Z7) scheme is suggested first by extending the method of Borges et al for the fifth-order WENO scheme. The sufficient condition for seventh-order accuracy is discussed only considering the new smoothness indicator. Then, the role of the parameter  $\varepsilon$ , which is used to construct the weights of WENO schemes to prevent the denominator from being zero, is discussed, and an optimized value of  $\varepsilon$  is suggested to improve the convergence and accuracy for 2D practical applications. Several examples are calculated to demonstrate the efficiency, robustness and accuracy of the methodology.

## 2 Weighted essentially non-oscillatory schemes

For the conservation law,

$$\frac{\partial u}{\partial t} + \frac{\partial f}{\partial x} = 0 \quad (1)$$

The semi-discretized form of Eq. (1) by using conservative finite difference formula can be written as

$$\frac{du_i(t)}{dt} = \frac{1}{\Delta x}(h_{i+\frac{1}{2}} - h_{i-\frac{1}{2}}) \quad (2)$$

The fluxes of WENO scheme are constructed through the convex combination of interpolated values  $\hat{f}^k(x_i \pm \frac{1}{2})$ , in which  $\hat{f}^k(x)$  is the  $r$ th-degree polynomial, defined as[1, 2, 7, 10]:

$$h_{i+\frac{1}{2}} = \sum_{k=0}^{r-1} \omega_k \hat{f}^k(x_{i+\frac{1}{2}}) \quad (3)$$

where

$$\hat{f}_{i+\frac{1}{2}}^k = \hat{f}^k(x_{i+\frac{1}{2}}) = \sum_{j=0}^{r-1} c_{kj} f_{i-k+j}, \quad i = 0, \dots, N \quad (4)$$

The weights  $\omega_k$  are defined as

$$\omega_k = \frac{\alpha_k}{\sum_{l=0}^{r-1} \alpha_l}, \quad \alpha_k = \frac{d_k}{(\beta_k + \varepsilon)^p} \quad (5)$$

The coefficient  $d_k$  are the optimal weights, which generate the  $(2r - 1)$ th order upstream central scheme. The coefficients of  $c_{kj}$  and  $d_k$  of  $r = 4$  for seventh-order WENO schemes[7] are listed in Table 1.

The smoothness indicators  $\beta_k$  suggested by Jiang and Shu[2] are given by

$$\beta_k = \sum_{l=1}^{r-1} \Delta x^{2l-1} \int_{x_{i-\frac{1}{2}}}^{x_{i+\frac{1}{2}}} \left( \frac{d^l}{dx^l} \hat{f}^k(x) \right)^2 dx \quad (6)$$

Table 1: Coefficients of  $c_{kj}$  and  $d_k$ 

$c_{kj}$	j=1	j=2	j=3	j=4	$d_k$
k=0	-1/4	13/12	-23/12	25/12	1/35
k=1	1/12	-5/12	13/12	1/4	12/35
k=2	-1/12	7/12	7/12	-1/12	18/35
k=3	1/4	13/12	-5/12	1/12	4/35

According the analysis of Henrick et al[9] and Borges et al[10], the necessary and sufficient conditions for  $(2r - 1)$ th order convergence in (3) are given as

$$\sum_{k=0}^{r-1} A_k(\omega_k^+ - \omega_k^-) = O(\Delta x^r) \quad (7)$$

$$\omega_k^\pm - d_k = O(\Delta x^{r-1}) \quad (8)$$

where  $A_k$  is the coefficient of Taylor series of  $\hat{f}_{i\pm 1/2}^k$ , it is independent of  $\Delta x$ . Superscripts  $\pm$  corresponds to the  $\pm$  in the  $\hat{f}_{i\pm 1/2}^k$ . A sufficient condition for  $(2r - 1)$ th order of convergence is given by [9, 10]

$$\omega_k^\pm - d_k = O(\Delta x^r) \quad (9)$$

For the fifth-order WENO scheme, a mapping function  $g_k(\omega)$  is proposed by Henrick et al[9] to make Eq. (9) be satisfied at critical points. However, if at a critical point the second derivative also vanishes, the WENO scheme of Henrick et al maintains the same second order of convergence as the classical WENO of Jiang and Shu[2]. Borges et al [10] used the whole 5-points stencil to devise a smoothness indicator, which has higher order than the classical smoothness indicators.

The smoothness indicators  $\beta_k^z$  defined by Borges et al [10] are

$$\beta_k^z = \frac{\beta_k + \varepsilon}{\beta_k + \tau_5 + \varepsilon}, \quad k = 0, 1, 2 \quad (10)$$

and the corresponding WENO weights  $\omega_k^z$  are

$$\omega_k^z = \frac{\alpha_k^z}{\sum_{l=0}^2 \alpha_l^z}, \quad \alpha_k^z = \frac{d_k}{\beta_k^z} = d_k[1 + (\frac{\tau_5}{\beta_k + \varepsilon})^q], \quad k = 0, 1, 2 \quad (11)$$

where

$$\tau_5 = |\beta_0 - \beta_2| \quad (12)$$

The parameter  $\varepsilon$  is used to avoid the division by zero and  $q$  are chosen to increase the difference of scales of distinct weights at non-smooth parts of the solution as  $p$  used in Eq. (5). For a smooth function, increasing the value of  $q$  makes the scheme closer to the optimal central upwind scheme. On the other hand, for a discontinuous solution, increasing  $q$  makes the scheme more dissipative[10].

The study of Borges et al [10] shows that their smoothness indicators  $\beta_k^z$  are higher order than the original  $\beta_k$  of Jiang and Shu's[2]. The resulted WENO scheme (WENO-Z) has less dissipation and higher resolution than Jiang and Shu's WENO scheme(WENO-JS).

From Eq.(6), there is

$$\tau_5 = \frac{13}{3}|f_i'' f_i'''| \Delta x^5 + O(\Delta x^6) \quad (13)$$

So, for the smooth solution,

$$\frac{\tau_5}{\beta_k} = O(\Delta x^3) \quad (14)$$

and from Eq.(11),

$$\omega_k^z = d_k + O(\Delta x^3) \quad (15)$$

At a critical point ( $f'_i = 0$ , but  $f''_i \neq 0$ ), the fifth order also can be achieved with  $q = 2$ [10].

Next, following the idea of Borges, an improved seventh-order WENO scheme is constructed.

### 3 An improved seventh-order WENO scheme

In this section, a new 7th-order WENO scheme (WENO-Z7) is extended following the idea of WENO-Z scheme proposed by Borges et al for the 5th-order WENO scheme[10]. For the 7th-order WENO scheme ( $r = 4$ ), the smoothness indicators  $\beta_k$  given by Balsara and Shu[7] are

$$\begin{aligned} \beta_0 &= f_{i-3}(547f_{i-3} - 3882f_{i-2} + 4642f_{i-1} - 1854f_i) + f_{i-2}(7043f_{i-2} - 17246f_{i-1} \\ &\quad + 7042f_i) + f_{i-1}(11003f_{i-1} - 9402f_i) + 2107f_i^2 \\ \beta_1 &= f_{i-2}(267f_{i-2} - 1642f_{i-1} + 1602f_i - 494f_{i+1}) + f_{i-1}(2843f_{i-1} - 5966f_i \\ &\quad + 1922f_{i+1}) + f_i(3443f_i - 2522f_{i+1}) + 547f_{i+1}^2 \\ \beta_2 &= f_{i-1}(547f_{i-1} - 2522f_i + 1922f_{i+1} - 494f_{i+2}) + f_i(3443f_i - 5966f_{i+1} \\ &\quad + 1602f_{i+2}) + f_{i+1}(2843f_{i+1} - 1642f_{i+2}) + 267f_{i+2}^2 \\ \beta_3 &= f_i(2107f_i - 9402f_{i+1} + 7042f_{i+2} - 1854f_{i+3}) + f_{i+1}(11003f_{i+1} - 17246f_{i+2} \\ &\quad + 4642f_{i+3}) + f_{i+2}(7043f_{i+2} - 3882f_{i+3}) + 547f_{i+3}^2 \end{aligned} \quad (16)$$

and they can be rewritten as[19]:

$$\beta_k = \sum_{l=1}^{r-1} \gamma_l [f_i^{(l)}(i+k-r+1, \dots, i+k) \Delta x^l]^2 \quad (17)$$

where

$$\gamma_1 = 240, \quad \gamma_2 = 1040, \quad \gamma_3 = 9372, \quad (18)$$

and  $f_i^{(l)}(i+k-r+1, \dots, i+k)$  denotes the differencing approximation of  $l$ th order derivative  $f_i^{(l)}$  by using points  $x_{i+k-r+1}, \dots, x_{i+k}$ . Because  $r$  points are used, the highest order approximation of  $f_i^{(l)}$  is  $(r-l)$ th order interpolation.

Taylor expansion of  $\beta_k$  gives

$$\begin{cases} \beta_0 = \gamma_1 [f'_i \Delta x - \frac{6}{4!} f_i^{(4)} \Delta x^4 + O(\Delta x^5)]^2 + \gamma_2 [f''_i \Delta x^2 + O(\Delta x^4)]^2 + \gamma_3 [f'''_i \Delta x^3 - \frac{6}{4!} f_i^{(4)} \Delta x^4 + O(\Delta x^5)]^2 \\ \beta_1 = \gamma_1 [f'_i \Delta x + \frac{2}{4!} f_i^{(4)} \Delta x^4 + O(\Delta x^5)]^2 + \gamma_2 [f''_i \Delta x^2 + O(\Delta x^4)]^2 + \gamma_3 [f'''_i \Delta x^3 - \frac{2}{4!} f_i^{(4)} \Delta x^4 + O(\Delta x^5)]^2 \\ \beta_2 = \gamma_1 [f'_i \Delta x - \frac{2}{4!} f_i^{(4)} \Delta x^4 + O(\Delta x^5)]^2 + \gamma_2 [f''_i \Delta x^2 + O(\Delta x^4)]^2 + \gamma_3 [f'''_i \Delta x^3 + \frac{2}{4!} f_i^{(4)} \Delta x^4 + O(\Delta x^5)]^2 \\ \beta_3 = \gamma_1 [f'_i \Delta x + \frac{6}{4!} f_i^{(4)} \Delta x^4 + O(\Delta x^5)]^2 + \gamma_2 [f''_i \Delta x^2 + O(\Delta x^4)]^2 + \gamma_3 [f'''_i \Delta x^3 + \frac{6}{4!} f_i^{(4)} \Delta x^4 + O(\Delta x^5)]^2 \end{cases} \quad (19)$$

Hence, there is

$$\beta_k = D(1 + O(\Delta x^2)), \text{ if } f'_i \neq 0 \text{ or } f''_i \neq 0, \quad (20)$$

this results in

$$\omega_k = d_k + O(\Delta x^2),$$

which does not satisfy the necessary and sufficient conditions (7) and (8) for seventh-order accuracy ( $r = 4$ ).

Following the method of Borges et al for the fifth-order WENO scheme[10], a new parameter  $\tau_7$  is introduced as

$$\tau_7 = |\beta_0 - \beta_3| \quad (21)$$

And the new 7th-order WENO weights  $\omega_k^z$  is defined as

$$\omega_k^z = \frac{\alpha_k^z}{\sum_{l=0}^3 \alpha_l^z}, \quad \alpha_k^z = d_k [1 + (\frac{\tau_7}{\beta_k + \varepsilon})^q] \quad (22)$$

From the Taylor expansions of  $\beta_k$ , there is

$$\tau_7 = \begin{cases} \frac{1}{2}\gamma_3 |f_i''' f_i^{(4)}| \Delta x^7 + O(\Delta x^8), & f' = 0 \text{ and } f'' = 0 \\ \frac{1}{2}\gamma_1 |f_i' f_i^{(4)}| \Delta x^5 + O(\Delta x^6), & \text{otherwise} \end{cases} \quad (23)$$

Hence

$$(1 + \frac{\tau_7}{\beta_k}) = \begin{cases} 1 + O(\Delta x^3), & f_i' \neq 0, \\ 1 + O(\Delta x^2), & f_i' = 0 \text{ and } f_i'' \neq 0, \\ 1 + O(\Delta x), & f_i' = 0 \text{ and } f_i'' = 0, \end{cases} \quad (24)$$

and from (11),

$$\omega_k^z = \begin{cases} d_k + O(\Delta x^3)^q, & f_i' \neq 0, \\ d_k + O(\Delta x^2)^q, & f_i' = 0 \text{ and } f_i'' \neq 0, \\ d_k + O(\Delta x)^q, & f_i' = 0, f_i'' = 0, \text{ and } f_i''' \neq 0, \end{cases} \quad (25)$$

Clearly, the sufficient condition of Eq. (9) is satisfied under the following conditions: (1)  $q \geq 4/3$  if  $f_i' \neq 0$ ; (2) at critical points ( $f_i' = 0$ ),  $q = 2$  if  $f_i'' \neq 0$ , or  $q \geq 4$  if  $f_i'' = 0$  and  $f_i''' \neq 0$ . That is, the improved WENO-Z7 scheme achieves seventh-order accuracy under these conditions.

## 4 The Role of $\varepsilon$

The different roles of  $\varepsilon$  are discussed in [9] and in[20]. Based on the point view of Henrick et al[9], since the oscillations of order  $\varepsilon^2$  can exist near discontinuities, choosing a  $\varepsilon$  which is too large mitigates the ENO behavior of WENO scheme. Meanwhile, as  $\varepsilon$  becomes the dominant term in  $\beta_k + \varepsilon$ , the smoothness indicator becomes inconsequential, and the preconditions of WENO scheme approach those of central upwind difference scheme. Henrick et al suggest that  $\varepsilon$  should be slightly larger than the square root of the smallest positive number allowed for a particular machine.

However, Shen et al[20] observed that, in practical applications, the mesh size  $\Delta x$  can not be infinite, and the flow fields do not vary uniformly. Hence, even for very smooth flow fields, there always exist difference between the smoothness indicators  $\beta_k$  and disturbance in the calculation of  $\beta_k$ . In most of the situations, the difference or disturbance induces the weights oscillation, and results in convergence problem, and decreases the numerical accuracy. Shen et al[20] suggested an optimized  $\varepsilon$  value of  $10^{-2}$  to remove the weights oscillation, improve convergence, and minimize the numerical dissipation.

In this paper, the studies of two dimensional flow applications find that the convergence problem of the seventh-order WENO schemes also exists. Different  $\varepsilon$  values of  $10^{-6}$  and  $10^{-2}$  are applied to compare the behavior of the seventh-order WENO schemes. The numerical results show that  $\varepsilon = 10^{-2}$  does actually improve the convergence, accuracy and robustness of the WENO schemes.

However, the  $\varepsilon = 10^{-2}$  is relative in scale to the normalized smoothness indicator defined as

$$\beta'_k = \beta_k / \gamma_1$$

where  $\beta_k$  is defined as Eq. (16) or (17),  $\gamma_1$  is the coefficient of the first derivative in the Taylor expansion of smoothness indicator, for example, Eq. (17) or (19). Hence, in all calculations in this paper,  $\beta'_k$  is used instead of  $\beta_k$ .

Table 2: Accuracy of  $f'(x)$ ,  $f(x) = x^3 + \cos(x)$ 

$\Delta x$	WENO-BS		WENO-Z7,q=1		WENO-Z7,q=2		WENO-Z7,q=4	
	Error	Ord	Error	Ord	Error	Ord	Error	Ord
.50000	.770E-04		.250E-04		.273E-04		.246E-04	
.25000	.816E-05	3.24	.590E-06	5.40	.358E-06	6.25	.224E-06	6.78
.12500	.385E-06	4.41	.134E-07	5.46	.325E-08	6.78	.171E-08	7.04
.06250	.142E-07	4.76	.495E-10	8.08	.136E-10	7.89	.133E-10	7.00
.03125	.436E-09	5.02	.213E-12	7.86	.114E-12	6.90	.112E-12	6.89

## 5 Numerical Examples

### 5.1 The Accuracy Testing of 1-D Problems

In this section, the 4th order Runge-Kutta-type method[21] is used for the time integration.  $\varepsilon = 10^{-20}$  is used for Eqs. (5) and (22).

#### 5.1.1 The error and rate of convergence for $f(x) = x^3 + \cos(x)$

First, the function  $f(x) = x^3 + \cos(x)$ [10], which has the first-order critical point at  $x = 0$ , is calculated to test the error and rate of convergence for the above schemes. Table 2 shows the  $L_\infty$  error and rate of convergence of  $f(x)$ . It can be seen that, if  $q$  equals 2 and 4, the rate of convergence of the WENO-Z7 scheme achieves 7th order; if  $q$  equals 1, the WENO-Z7 scheme with coarse grid is only 5th order. The WENO-BS has achieved only 5th-order accuracy. It is worse with coarse grid.

#### 5.1.2 Linear transport equation

The linear transport equation is used to test the accuracy of WENO schemes. In this paper,  $CFL = 0.5$  and  $q = 2$  are used unless otherwise specified.

$$\frac{\partial u}{\partial t} + \frac{\partial u}{\partial x} = 0, \quad -1 < x < 1 \quad (26)$$

$$u(x, 0) = u_0(x), \text{ periodic}$$

#### (1) Initial solution $u_0(x) = \sin(\pi x)$

Table 3 gives the errors and accuracy order of the wave equation with the initial solution of  $\sin(n\pi)$ . It can be seen that, for this smooth solution, the 7th-order WENO-Z7 scheme obtains almost the same results and accuracy order as the seventh-order upstream central scheme. It is more accurate than the 7th-order WENO-BS scheme as expected.

#### (2) Initial solution

$$u_0(x) = \begin{cases} -x\sin(3\pi x^2/2), & -1 \leq x < -1/3 \\ |\sin(2\pi x)|, & -1/3 \leq x \leq 1/3 \\ 2x - 1 - \sin(3\pi x)/6, & \text{otherwise} \end{cases} \quad (27)$$

Figs. 1 shows the numerical solutions at  $t = 6$ . The present WENO-Z7 scheme resolves discontinuities better than the WENO-BS scheme.

Table 3: Accuracy on  $u_t + u_x = 0$  with  $u_0(x) = \sin(\pi x)$ ,  $t=1$ 

Scheme	$N$	$L_\infty$ error	$L_\infty$ order	$L_1$ error	$L_1$ order
WENO-BS	10	0.206031E+00	—	0.136799E+00	—
	20	0.878497E-02	4.552	0.384864E-02	5.152
	40	0.225660E-03	5.283	0.851062E-04	5.499
	80	0.541237E-05	5.382	0.122066E-05	6.124
	160	0.148036E-06	5.192	0.184780E-07	6.046
WENO-Z7	10	0.275615E+00	—	0.171290E+00	—
	20	0.120747E-02	7.835	0.564025E-03	8.246
	40	0.684514E-05	7.463	0.415478E-05	7.085
	80	0.534323E-07	7.001	0.334013E-07	6.959
	160	0.465962E-09	6.841	0.296040E-09	6.818
7th-order upstream central	10	0.723497E-01	—	0.459978E-01	—
	20	0.790217E-03	6.517	0.497473E-03	6.531
	40	0.655931E-05	6.913	0.415893E-05	6.902
	80	0.529833E-07	6.952	0.334014E-07	6.960
	160	0.465975E-09	6.829	0.296041E-09	6.818

### (3) Initial solution

$$u_0(x) = \begin{cases} \frac{1}{6}(G(x, \beta, z - \delta) + G(x, \beta, z + \delta) + 4G(x, \beta, z)), & -0.8 \leq x \leq -0.6, \\ 1, & -0.4 \leq x \leq -0.2, \\ 1 - |10(x - 0.1)|, & 0 \leq x \leq 0.2, \\ \frac{1}{6}(F(x, \alpha, \alpha - \delta) + F(x, \alpha, \alpha + \delta) + 4F(x, \alpha, a)), & 0.4 \leq x \leq 0.6, \\ 0, & \text{otherwise} \end{cases} \quad (28)$$

As in Ref.[2], the constants for this case are taken as  $a = 0.5$ ,  $z = -0.7$ ,  $\delta = 0.005$ ,  $\alpha = 10$ , and  $\beta = \log 2 / 36 \delta^2$ . The solution contains a smooth combination of Gaussians, a square wave, a sharp triangle wave, and a half ellipse.

The results at  $t = 8$  with 200 grid points are shown in Figs. 2 and 3. It can be seen that the WENO-Z7 with  $q = 1$  obtains more accurately resolved solution than the WENO-BS. It is worth pointing out that, with  $q = 2$ , the WENO-Z7 scheme can obtain more accurate solution for the three wave of Gaussians, a square wave, a sharp triangle wave. However, for the half ellipse wave, the WENO-BS is better.

#### 5.1.3 Nonlinear Transport Equation

The nonlinear transport equation can be written as

$$\frac{\partial u}{\partial t} + u \frac{\partial u}{\partial x} = 0, \quad 0 \leq x \leq 2\pi$$

with initial and boundary conditions

$$u_0(x) = 0.3 + 0.7 \sin(x), \quad 0 \leq x \leq 2\pi, \quad \text{periodic}$$

The Lax-Friedrichs splitting method is used, in which  $f^\pm = \frac{1}{2}(f(u) \pm au)$ ,  $f(u) = \frac{1}{2}u^2$ , and  $a = \max_u |f'(u)|$ . Fig. 4 shows the results at  $t = 2$  with grid number of  $N = 80$ . The WENO-Z7 and WENO-BS schemes obtain almost the identical non-oscillatory solutions.

### 5.1.4 1D Shock Wave Tube, Sod Problem

To examine the new scheme for nonlinear equations, the one-dimensional Euler equations are solved for the 1D shock tube problem. Again, the 4th order Runge-Kutta method is used for time marching.

1D Euler equations:

$$\frac{\partial \mathbf{U}}{\partial t} + \frac{\partial \mathbf{F}}{\partial x} = 0 \quad (29)$$

where

$$\mathbf{U} = \begin{bmatrix} \rho \\ \rho u \\ \rho e \end{bmatrix}, \quad \mathbf{F} = \begin{bmatrix} \rho u \\ \rho u^2 + p \\ u(\rho e + p) \end{bmatrix}, \quad p = (\gamma - 1)(\rho e - \rho u^2/2), \quad \gamma = 1.4.$$

The initial condition is

$$(\rho, u, p) = \begin{cases} (1.0, 0.0, 1.0), & x \leq 7.5, \\ (0.125, 0.0, 0.1), & x > 7.5. \end{cases} \quad (30)$$

In this case, the Roe's Riemann solver is used. The grid points is  $N = 200$ . Fig. 5 gives the density and velocity distributions. Both the WENO-BS and present WENO-Z7 schemes have slight oscillation near the contact discontinuity. They all can capture expansion wave and shock wave accurately.

### 5.1.5 1D Shock Wave Tube, Shu-Osher Problem

This problem is governed by the one-dimensional Euler equations (29) with following initial condition:

$$(\rho, u, p) = \begin{cases} (3.857143, 2.629369, 10.3333), & \text{when } x < -4, \\ (1 + \varepsilon \sin(5x), 0.0, 1.0), & \text{when } x \geq -4. \end{cases} \quad (31)$$

where,  $\varepsilon = 0.2$ . This case represents a Mach 3 shock wave interacting with a sine entropy wave[4]. The results at time  $t = 1.8$  are plotted in Figs. 6. The "exact" solutions are the numerical solutions of the original WENO-5 scheme with grid points of  $N = 8000$ . For this case, the present WENO-Z7 scheme achieves more accurate result than the WENO-BS scheme.

## 5.2 Applications to 2-D Flows

The normalized Navier-Stokes equations governing compressible viscous flows can be written in the Cartesian coordinate as:

$$\frac{\partial U}{\partial t} + \frac{\partial E}{\partial x} + \frac{\partial F}{\partial y} + \frac{\partial G}{\partial z} = \frac{1}{Re} \left( \frac{\partial R}{\partial x} + \frac{\partial S}{\partial y} + \frac{\partial T}{\partial z} \right) \quad (32)$$

where

$$U = \begin{bmatrix} \rho \\ \rho u \\ \rho v \\ \rho w \\ \rho e \end{bmatrix}, \quad E = \begin{bmatrix} \rho u \\ \rho u^2 + p \\ \rho uv \\ \rho uw \\ (\rho e + p)u \end{bmatrix}, \quad F = \begin{bmatrix} \rho v \\ \rho uv \\ \rho v^2 + p \\ \rho vw \\ (\rho e + p)v \end{bmatrix}, \quad G = \begin{bmatrix} \rho w \\ \rho uw \\ \rho vw \\ \rho w^2 + p \\ (\rho e + p)w \end{bmatrix},$$

$$R = \begin{bmatrix} 0 \\ \tau_{xx} \\ \tau_{xy} \\ \tau_{xz} \\ u_k \tau_{xk} - q_x \end{bmatrix}, \quad S = \begin{bmatrix} 0 \\ \tau_{xy} \\ \tau_{yy} \\ \tau_{yz} \\ u_k \tau_{yk} - q_y \end{bmatrix}, \quad T = \begin{bmatrix} 0 \\ \tau_{xz} \\ \tau_{yz} \\ \tau_{zz} \\ u_k \tau_{zk} - q_z \end{bmatrix},$$



The repeated index  $k$  stands for the Einstein summation over  $x, y$  and  $z$ . The stress  $\tau$  and heat flux  $q$  are,

$$\tau_{ik} = (\mu + \mu_t) \left[ \left( \frac{\partial u_i}{\partial x_k} + \frac{\partial u_k}{\partial x_i} \right) - \frac{2}{3} \delta_{ik} \frac{\partial u_j}{\partial x_j} \right]$$

$$q_j = \frac{-1}{(\gamma - 1)M_\infty^2} \left( \frac{\mu}{Pr} + \frac{\mu_t}{Pr_t} \right) \frac{\partial T}{\partial x_j}$$

The equation of state is

$$\rho e = \frac{p}{\gamma - 1} + \frac{1}{2} \rho (u^2 + v^2 + w^2)$$

where  $\mu_t$  is the turbulence eddy viscosity calculated by Baldwin-Lomax(BL) model[22].

In the above equations,  $\rho$  is density,  $u, v$ , and  $w$  are the Cartesian velocity components in  $x, y$  and  $z$  directions,  $p$  is static pressure, and  $e$  is total energy per unit mass,  $\mu$  is molecular viscosity,  $J$  is the transformation Jacobian,  $\gamma, Re, M_\infty, Pr$  and  $Pr_t$  are the ratio of specific heat, Reynolds number, freestream Mach number, Prandtl number and turbulent Prandtl number, respectively.

In this paper, the sixth-order central differencing[23] is used for the discretization of viscous terms, and the unfactored implicit Gauss-Seidel line relaxation method[20, 24] is used for time integration.

### 5.2.1 Subsonic Flat Plate Turbulent Boundary Layer

The subsonic flat plate turbulent boundary layer is used as the first 2-D test example. In this case, the Baldwin-Lomax turbulence model is applied. The cell size is  $180 \times 80$ . The non-dimensional distance  $y^+$  of the first point to the wall is kept under 0.2. The inlet Mach number is 0.5, and the Reynolds number is  $4 \times 10^6$  based on the plate length. The flow is subsonic at inlet and outlet.

Fig. 7 shows the convergence histories of both WENO-Z7 scheme and WENO-BS scheme with different  $\varepsilon$  values. For this case, all the residuals can achieve machine zero, the convergence with  $\varepsilon = 10^{-2}$  is a little faster than that with  $\varepsilon = 10^{-6}$ . The velocity distribution shown in Fig. 8 shows that all results are in good agreement with the law of the wall.

### 5.2.2 Transonic Converging-Diverging Nozzle

To examine the performance of the new 7th order WENO scheme for capturing the weak shock waves that do not align with the mesh lines, the 2D Euler equations is solved for an inviscid transonic converging-diverging nozzle flow. The nozzle was designed and tested at NASA and was named as Nozzle A2[25]. The cell size is  $175 \times 80$ . The grid is clustered near the wall. The inlet Mach number is 0.22. CFL=3 is used.

Fig. 13 is the convergence histories. From this figure, it can be seen that, with  $\varepsilon = 10^{-6}$ , the residuals of both the present WENO-Z7 and the WENO-BS schemes are only around  $0.2 \times 10^{-1}$ . With  $\varepsilon = 10^{-2}$ , both schemes can achieve  $10^{-12}$ , but WENO-Z7 converges much faster than WENO-BS.

Fig. 10 are the pressure contours obtained by WENO-Z7 with  $\varepsilon = 10^{-6}$  and  $\varepsilon = 10^{-2}$ , respectively. They all can capture the shock waves well.

Fig. 11 is the distribution of the wall pressure coefficient. From the zoomed plot in Fig. 10, it can be seen that the schemes with  $\varepsilon = 10^{-2}$  resolve sharper shock waves with higher peak values. This also indicates that the not well converged solutions may decrease the resolution of the numerical results.

### 5.2.3 Transonic RAE2822 Airfoil

The steady state solution of the transonic RAE2822 airfoil is calculated using the new 7th order WENO schemes with Reynolds averaged NS equation. The Baldwin-Lomax turbulent model is used. The computational region is divided into two blocks, and the mesh size of  $128 \times 55$  is used for each block, the freestream Mach number  $M_\infty$  is 0.729, the Reynolds number based on chord is  $6.5 \times 10^6$ , and the angle of attack is  $2.31^\circ$ . CFL=3 is used.

Fig. 13 is the convergence histories. Similarly, with  $\varepsilon = 10^{-6}$ , the residuals of WENO-BS and WENO-Z7 remain  $0.2 \times 10^{-3}$  and  $0.1 \times 10^{-2}$ , respectively. However, with  $\varepsilon = 10^{-2}$ , both schemes can achieve very low level residual, even though with small oscillation.

Figs. 14 and 15 are the comparisons of the pressure coefficient and the skin friction coefficient, respectively. All results are in good agreement with the experiment. Figs. 16 and 17 are the pressure contours showing the shock captured on the suction surface. This case shows the robustness of the new 7th order WENO scheme to resolve a practical transonic flow with shock boundary layer interaction. The applications for more complex flow fields are currently underway.

## 6 Conclusions

This paper gives the following conclusions:

- (1) An improved seventh-order WENO (WENO-Z7) scheme is constructed by extending the methodology of Borges et al[10] for fifth-order WENO schemes. Using the new suggested smoothness indicator, the sufficient condition for seventh-order accuracy is satisfied.
- (2) The role of the parameter  $\varepsilon$  is discussed. Since  $\varepsilon$  always appears with the smoothness indicator, it is naturally required that  $\varepsilon$  has the minimal effect on the weights, especially near shock waves. The view point of Henrick et al[9] is that the  $\varepsilon$  should be as small as possible. However, in smooth regions, it is crucial that the weights are not affected by the small disturbance of the smoothness indicator since the weights oscillation cause the convergence problem and decrease numerical accuracy. Hence, an enlarged and optimized[20]  $\varepsilon$  value of  $10^{-2}$  is suggested to improve the convergence and accuracy of the seventh-order WENO scheme for practical applications.

The 1D and 2D numerical examples show that the scheme is stable, accurate and robust.

## 7 Acknowledgment

This research is funded by the GUIde IV consortium grant 09-1010 and by AFOSR grant FA9550-09-1-0105.

## References

- [1] X.D. Liu, S. Osher, and T. Chan, "Weighted essentially non-oscillatory schemes," *J.Comput.Phys.*, vol. 115, pp. 200–212, 1994.
- [2] G.S. Jiang, and C.W. Shu, "Efficient implementation of weighted ENO schemes," *J.Comput.Phys.*, vol. 126, pp. 202–228, 1996.
- [3] A. Harten, B. Engquist, S. Osher, and S. Chakravarthy, "Uniformly High Order Essentially Non-Oscillatory Schemes, III," *Journal of Computational Physics*, vol. 71, pp. 231–303, 1987.

- [4] C.-W. Shu and O. Osher, “Efficient Implementation of Essentially Non-Oscillatory Shock Capturing Schemes, II,” *Journal of Computational Physics*, vol. 83, pp. 32–78, 1989.
- [5] Z.J. Wang and R.F. Chen, “Optimized weighted essentially non-oscillatory schemes for linear waves with discontinuity,” *J.Comput.Phys.*, vol. 174, pp. 381–404, 2001.
- [6] D. Ponziani, S. Pirozzoli, F. Grasso, “Development of optimized weighted-ENO schemes for multiscale compressible flows,” *Inter.J.Numer.Meth.Fluids*, vol. 42, pp. 953–977, 2003.
- [7] D.S. Balsara and C.-W. Shu, “Monotonicity Preserving weighted essentially non-oscillatory schemes with increasingly high order of accuracy,” *J.Comput.Phys.*, vol. 160, pp. 405–452, 2000.
- [8] Z.F. Xu and C.-W. Shu, “Anti-diffusive flux corrections for high order finite difference WENO schemes,” *J.Comput.Phys.*, vol. 205, pp. 458–485, 2005.
- [9] A.K. Henrick, T.D. Aslam, J.M. Powers, “Mapped weighted essentially non-oscillatory schemes: Achieving optimal order near critical points,” *J.Comput.Phys.*, vol. 208, pp. 206–227, 2005.
- [10] R. Borges, M. Carmona, B. Costa and W.S. Don, “An improved weighted essentially non-oscillatory scheme for hyperbolic conservation laws,” *Journal of Computational Physics*, vol. 227, pp. 3191–3211, 2008.
- [11] Y. Q. Shen and G. C. Zha, “Improvement of weighted essentially non-oscillatory schemes near discontinuity.” AIAA paper 2009-3655, 2009.
- [12] M. P. Martin, E. M. Taylor, M. Wu, and V. G. Weirs, “A Bandwidth-Optimized WENO Scheme for the Direct Numerical Simulation of Compressible Turbulence,” *Journal of Computational Physics*, vol. 220, pp. 270–289, 2006.
- [13] S. Pirozzoli, “Conservative hybrid compact-WENO schemes for shock-turbulence interaction,” *J.Comput.Phys.*, vol. 178, pp. 81–117, 2002.
- [14] D. Kim and J.H. Kwon, “A high-order accurate hybrid scheme using a central flux scheme and a WENO scheme for compressible flowfield analysis,” *J.Comput.Phys.*, vol. 210, pp. 554–583, 2005.
- [15] Y.Q. Shen and G.W. Yang, “Hybrid finite compact-WENO schemes for shock calculation,” *International Journal for Numerical Methods in Fluids*, vol. 53, pp. 531–560, 2007.
- [16] B. Costa and W. S. Don, “Multi-domain hybrid spectral-WENO methods for hyperbolic conservation laws,” *Journal of Computational Physics*, vol. 224, pp. 970–991, 2007.
- [17] B. Costa and W. S. Don, “High order Hybrid central-WENO finite difference scheme for conservation laws,” *Journal of Computational and Applied Mathematics*, vol. 204, pp. 209–218, 2007.
- [18] Y.Q. Shen, B.Y. Wang, and G.C. Zha, “Implicit WENO scheme and high order viscous formulas for compressible flows.” AIAA-2007-4431, June 2007.
- [19] Y. Q. Shen, G.-C. Zha, “A Robust Seventh-order WENO Scheme and Its Applications.” AIAA-2008-0757, 2008.
- [20] Y.-Q. Shen, G.-C. Zha, and B.-Y. Wang, “Improvement of Stability and Accuracy of Implicit WENO Scheme,” *AIAA Journal*, vol. 47, pp. 331–344, 2009.
- [21] Shu, C.-W. and Osher, O., “Efficient Implementation of Essentially Non-Oscillatory Shock Capturing Schemes,” *Journal of Computational Physics*, vol. 77, pp. 439–471, 1988.
- [22] B. Baldwin and H. Lomax, “Thin Layer Approximation and Algebraic Model for Separated Turbulent Flows.” AIAA Paper 78-257, 1978.

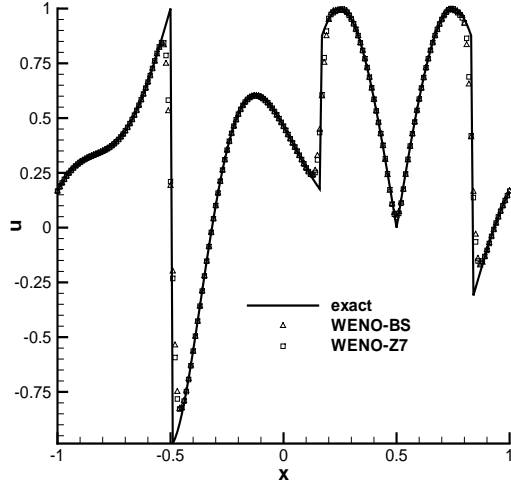


Figure 1: Numerical results,  $t=6$

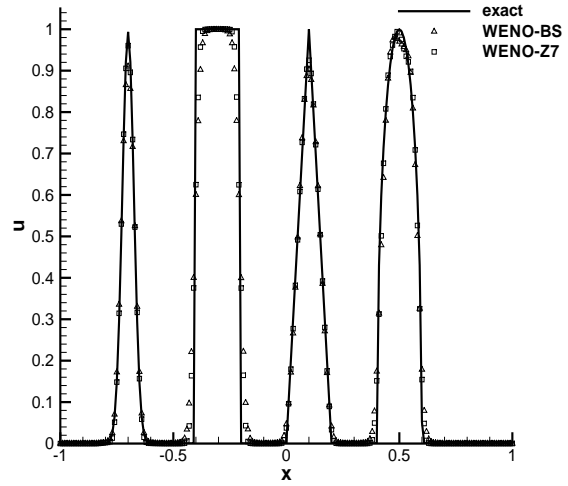


Figure 2: Numerical results,  $T=8$

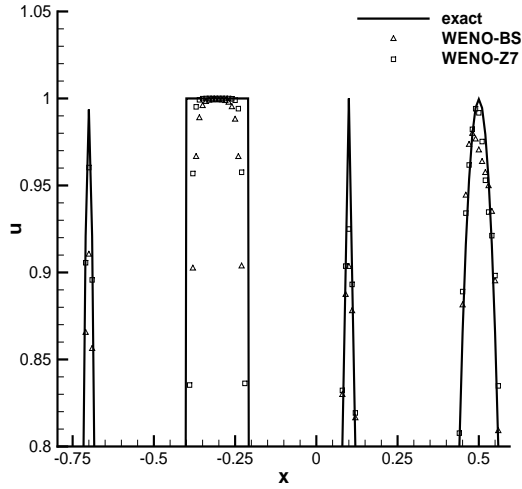


Figure 3: Locally enlarged plot of Fig. 2

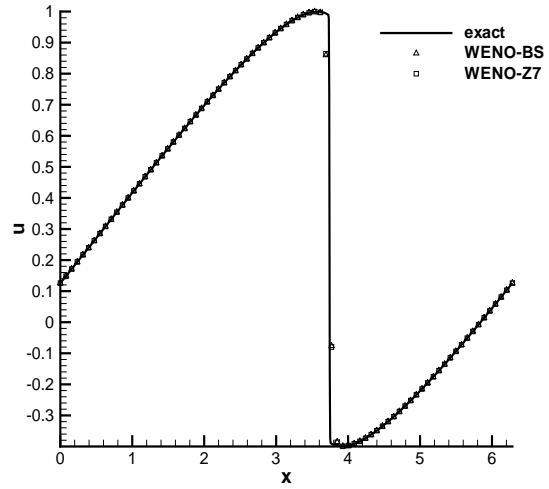


Figure 4: Numerical results,  $T=2$

- [23] Y.-Q. Shen and G.-C. Zha, "Comparison of High Order Schemes for Large Eddy Simulation of Circular Cylinder Flow." AIAA-2009-0945, 47th AIAA Aerospace Sciences Meeting and Exhibit, Orlando, FL, Jan. 5-8, 2009.
- [24] Y.Q. Shen, B.Y. Wang, and G.C. Zha, "Comparison Study of Implicit Gauss-Seidel Line Iteration Method for Transonic Flows." AIAA-2007-4332, June 2007.
- [25] Mason, M. L. and Putnam, L. E. , "The Effect of Throat Contouring on Two-Dimensional Converging-Diverging Nozzles at Static Conditions ." NASA Technical Paper 1704, 1980.

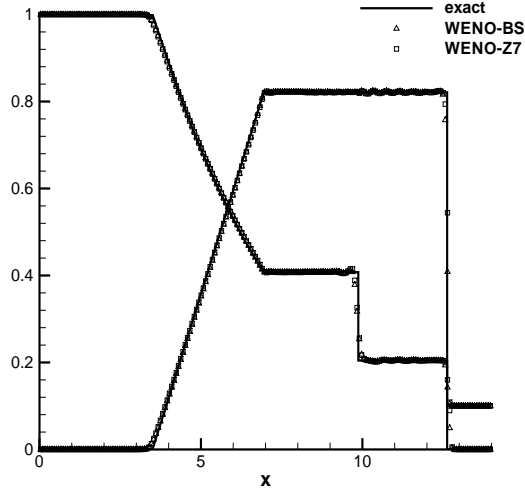


Figure 5: Density distribution, Sod problem

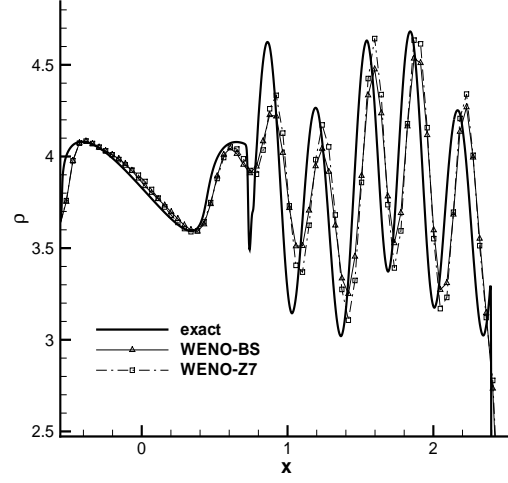


Figure 6: Density, Shu-Osher problem

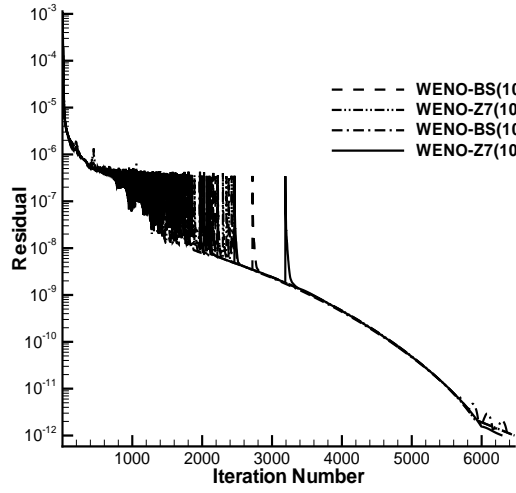


Figure 7: Convergence histories of the subsonic turbulent boundary layer flow

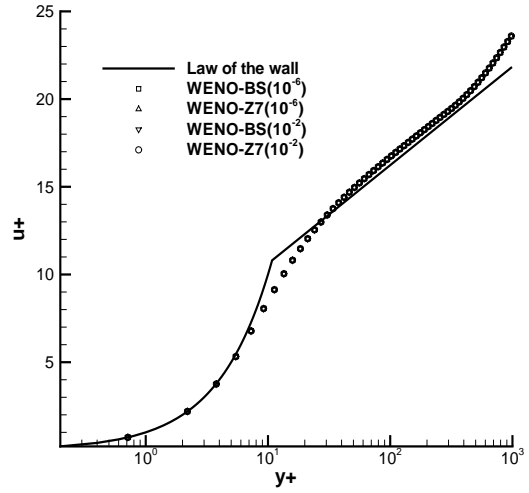


Figure 8: Velocity profiles of the subsonic turbulent boundary layer flow

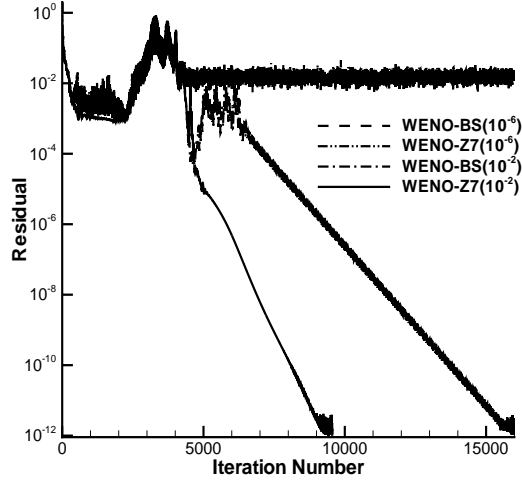


Figure 9: Convergence histories of the transonic converging-diverging nozzle flows

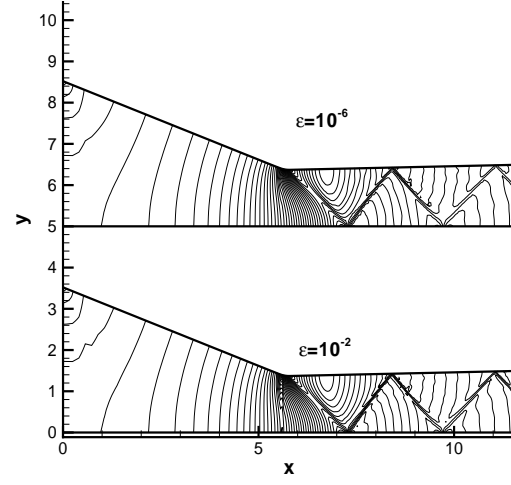


Figure 10: The pressure contours of the transonic converging-diverging nozzle flows, WENO-Z7

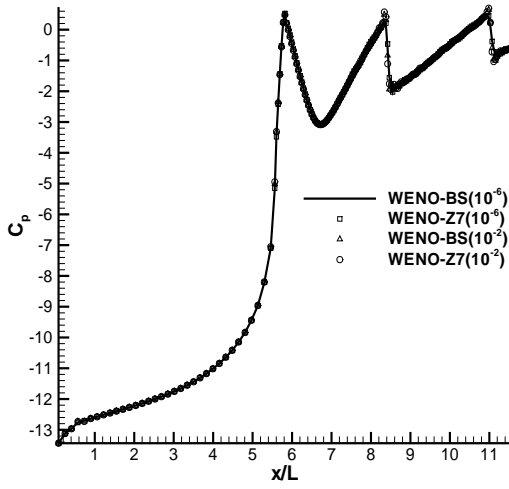


Figure 11: The pressure coefficients at the upper wall of the transonic converging-diverging nozzle flows

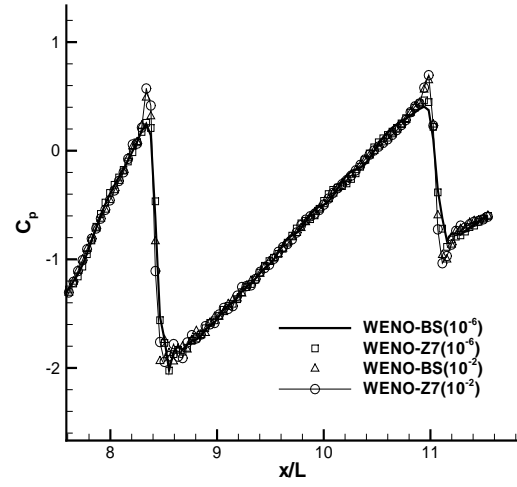


Figure 12: Zoomed plot of Fig. 11

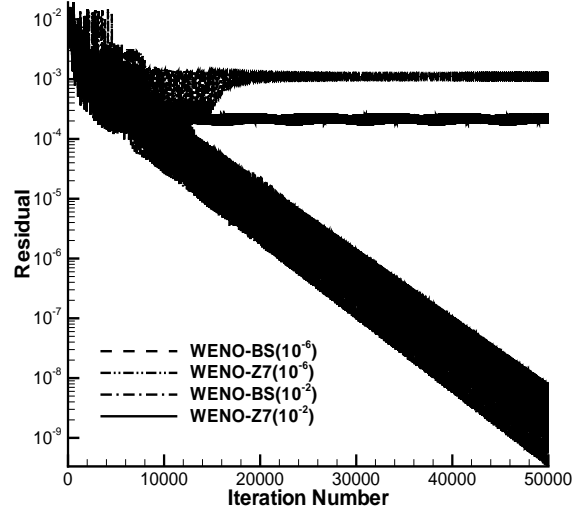


Figure 13: Convergence histories of the transonic flow for RAE2822 airfoil.

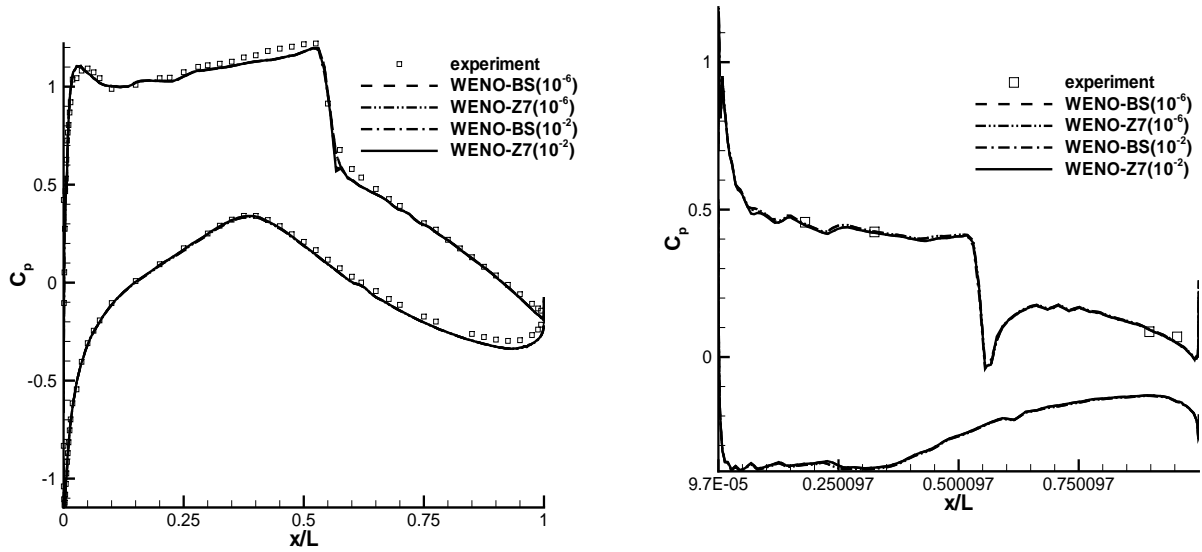


Figure 14: The pressure coefficients at the airfoil surface of the transonic flow for RAE2822 airfoil. Figure 15: The skin friction coefficients at the airfoil surface of the transonic flow for RAE2822 airfoil.

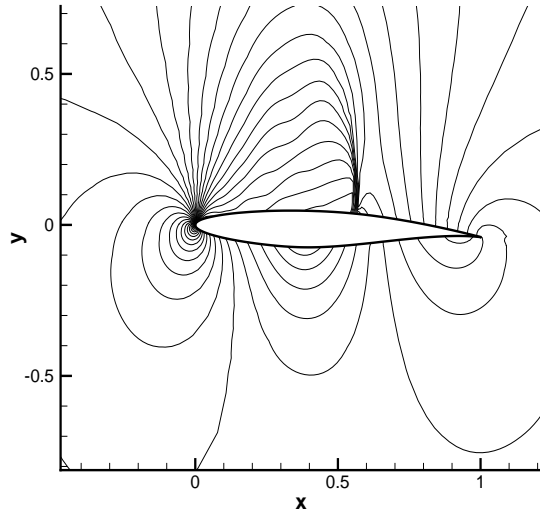


Figure 16: The pressure contours of the transonic flow for RAE2822 airfoil, WENO-Z7,  $\varepsilon = 10^{-6}$

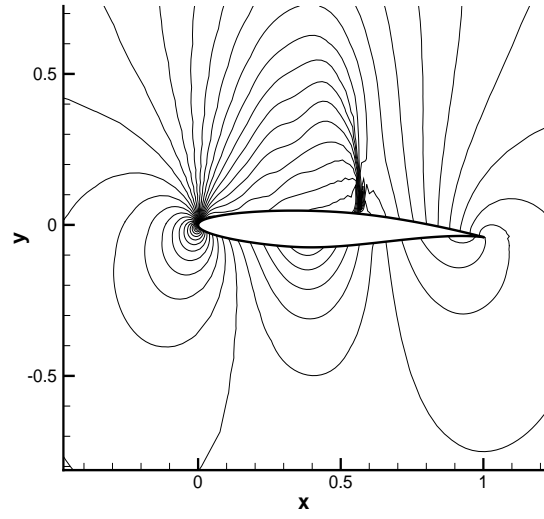


Figure 17: The pressure contours of the transonic flow for RAE2822 airfoil, WENO-Z7,  $\varepsilon = 10^{-2}$